Document downloaded from:

http://hdl.handle.net/10251/125572

This paper must be cited as:

Bares-Moreno, P.; Selmanaj, D.; Guardiola, C.; Onder, C. (2018). Knock probability estimation through an in-cylinder temperature model with exogenous noise. Mechanical Systems and Signal Processing. 98:756-769. https://doi.org/10.1016/j.ymssp.2017.05.033

The final publication is available at

http://doi.org/10.1016/j.ymssp.2017.05.033

Copyright Elsevier

Additional Information

*Manuscript
Click here to view linked References

Knock probability estimation through an in-cylinder temperature model with exogenous noise

P. Bares[1] * D. Selmanaj[2] C. Guardiola[1] C. Onder[2]

Universitat politècnica de València [1]
Swiss Federal Institute of Technology (ETH) [2]

Abstract

This paper presents a new knock model which combines a deterministic knock model based on the in-cylinder temperature and an exogenous noise disturbing this temperature. The autoignition of the end-gas is modelled by an Arrhenius-like function and the knock probability is estimated by propagating a virtual error probability distribution. Results show that the random nature of knock can be explained by uncertainties at the in-cylinder temperature estimation. The model only has one parameter for calibration and thus can be easily adapted online.

In order to reduce the measurement uncertainties associated with the air mass flow sensor, the trapped mass is derived from the in-cylinder pressure resonance, which improves the knock probability estimation and reduces the number of sensors needed for the model.

A four stroke SI engine was used for model validation. By varying the intake temperature, the engine speed, the injected fuel mass, and the spark advance, specific tests were conducted, which furnished data with various knock intensities and probabilities. The new model is able to predict the knock probability within a sufficient range at various operating conditions. The trapped mass obtained by the acoustical model was compared in steady conditions by using a fuel balance and a lambda sensor and differences below 1% were found.

Key words: Knock, SI engines, STFT, resonance, control

* Corresponding author:
Email address: pabamo@mot.upv.es (P. Bares[1]).

1 Introduction

In spark-ignited (SI) engines the combustion is initiated by the energy released by the spark. This combustion generates a flame front which moves along all the cylinder volume in a uniform manner [1]. During the flame propagation the temperature of the unburned gas increases due to the rise of the in-cylinder pressure. In normal combustion events, the flame front reaches all of the cylinder volume in a controlled scheme; however, high unburned gas temperatures can cause the autoignition of the end-gas.

The autoignition of the end-gas (knock) is an undesirable phenomenon and is one of the main limitations in SI engines. The rapid combustion of the end-gas heavily excites cylinder head resonance, and its vibration reduces the combustion efficiency and can damage the engine [2, 3, 4].

Current approaches for knock control use the spark advance (SA) timing for modifying the combustion phasing and thus, the likelihood of knock. The control strategies can be divided into two groups: stochastic and model-based. Stochastic methods aim to directly control the knock probability by varying the SA [5, 6, 7], while model-based methodologies use the spark advance for keeping in-cylinder conditions, e.g. un-burned gas temperature, within a desired range [8, 9, 10].

Regarding the physics behind the knock phenomenon, several studies state that knock cannot be predicted in a deterministic manner [11, 12]. One one hand, when operating in steady-state conditions, the flame propagation in SI combustion has a significant cycle-to-cycle variability [13, 14], which directly influences the cycle-to-cycle knock probability. On the other hand, some research suggest that the autoignition of the end-gas could be initiated at hot spots, influenced by inhomogeneities of the mixture [15, 16, 17]. Furthermore, the autoignition of the end-gas is driven by an Arrhenius-like function [18, 19], and small errors in the gas temperature are propagated in knock models by an exponential function resulting in important errors in the prediction of knock.

The present paper proposes estimating the knock probability by adding an exogenous noise over the in-cylinder temperature model. This noise represents uncertainties such as temperature hot spots, in-cylinder pressure pegging, wall heat transfer, residual mass variations, and sensor errors. Hence, the model is developed with the assumption that the random nature of knock is due only to in-cylinder temperature uncertainties. It is beyond the scope of this paper

to prove this assumption; however, the experimental results show that it improves the prediction capabilities of a control-oriented knock model.

The model presented aims to reduce the unburned gas uncertainties estimating the trapped mass by identifying the resonant frequencies of the in-cylinder pressure waves. The method was recently applied to DI and HCCI engines [20, 21, 22], and some applications, i.e. NOx and residual gas fraction estimation, have been already explored [23, 24]. One of the most important sources of error is the estimation of the trapped mass, which is a crucial parameter for the estimation of the unburned gas temperature. Measurement errors of hot-film air mass flow sensors, which are widely employed in automotive applications, can attain up to 20% because of ageing and other non-calibrated effects [25, 26]. Furthermore, there are no sensors for estimationg the residual gases, which in SI engines without negative valve overlap represent between 3 % and 5% of the total mass trapped, and they exhibit important cycle-by-cycle variations [27, 28].

In addition, past works on the method, as tested in cylinders with an in-piston bowl, do include the engine speed fluctuations with the bowl effect by a crank angle dependent parameter [29]. In this paper, a spark-ignited engine was used and the instantaneous engine speed was measured and modelled by the camshaft model given by Li and Stone in [30]. Herein, the frequency is demonstrated to follow Draper's equation [31] with no need for any calibration effort. A fuel balance, a lambda sensor, and a residual mass model were used for validation in steady conditions.

The resonance methodology is specially suitable for the knock modelling of SI engines for three reasons:

(1) SI engines normally do not have a bowl. Theory based on a cylindrical combustion chamber thus fits the physics better.
(2) Knocking conditions are produced at high loads, where combustion heavily excites the resonant frequencies, even in the absence of knock.
(3) SI combustion is performed in stoichiometric conditions and the resulting end-gas properties can be easily identified [32].

In order to evaluate the improvement associated with the methodology based on in-cylinder pressure for estimating the trapped mass, the knock model was run by using the trapped mass from the resonance method and by using the air mass flow sensor.

The paper is organized as follows: The next section introduces the experimental set-up and the tests performed. Section three describes the methodology for

determining the knock autoignition and Section four describes the procedure for estimating the knock probability by the addition of an exogenous noise. Section five shows the performance of the knock model and illustrates the effect of sensor errors by comparing the air mass flow sensor and the trapped mass obtained from resonance. Finally, the last section highlights the main contributions of the method and points out the future work required for using the model in a control scheme.

2 Experimental set-up

Tests were performed in a turbocharged four-stroke SI engine with 0.5 l of unitary displacement. The air-to-fuel ratio was maintained at stoichiometric conditions by controlling in a closed-loop the amount of fuel injected with a lambda sensor placed at the exhaust line. The air mass flow was measured by a hot-film anemometer and controlled by a waste-gate valve at the turbocharger. The main characteristics of the engine are summarized in Table 1.

Table 1
Main engine characteristics

	Units	Value
Cylinders	[-]	3
Combustion type	[-]	SI
Unitary displacement	[cc]	499.6
Bore	[mm]	82
Compression ratio	[-]	10.1:1

The engine was equipped with a variable valve timing (VVT) system and direct gasoline injection. The timing of the gasoline injection was set at 270 CAD before top dead center (TDC), the intake valve opening and closing (IVO and IVC) were set at 387 and 180 CAD before TDC, respectively, and the exhaust valve opening and closing (EVO and EVC) were set at 146 and 357 CAD after TDC. The two valve lift profiles are shown in Figure 1.

A fuel balance was used for fuel mass flow metering, which implies accurate measurements in steady-state conditions. Used in conjunction with a lambda sensor, this measurement provides an air mass flow estimation, as follows:

$$m_{air} = \lambda 14.7 m_{fuel} \tag{1}$$

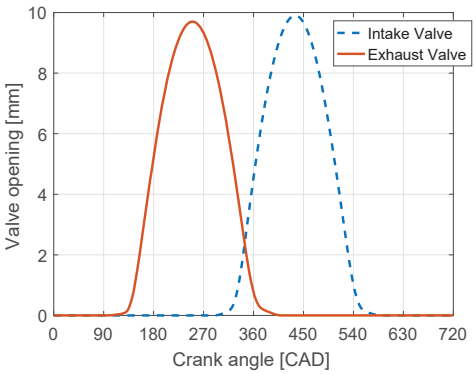

Fig. 1. Valves opening configuration

The residual gas fracion (RGF) was estimated from in-cylinder conditions at the EVO and EVC, such as several authors proposed [33, 34], as follows:

$$RGF = \left(\frac{V_{EVC}}{V_{EVO}}\right)\left(\frac{p_{EVC}}{p_{EVO}}\right)^{1/\gamma} \tag{2}$$

To analyse the pressure signals a short time Fourier transform (STFT) and Wigner distribution (WD) were used. The former uses the Fourier transform and a time-varying window to obtain the frequency spectrum with time resolution, while the latter multiplies the signal at a past time by the signal at a future time [35, 36, 37]. Each method has some advantages and disadvantages: On one hand, STFT is the most commonly used methodology as it is a robust method and does not require much computational time. However, STFT dilutes the signal by using a window function, which means that the frequency content obtained at instant t is affected by the surroundings. On the other hand, WD has a precise frequency spectrum, but ghost terms caused by artificial frequencies mask the real components. In this work Blackman-Harris window of 2.8 ms was used for STFT, while WD was implemented over the full signal.

Knock was detected by analysing the frequency content of the in-cylinder pressure signal such as in [38]. This methodology does detect low-knocking cycles by comparing the resonance excitation near the maximum heat release rate (normal combustion) and next to the maximum unburned temperature (autoignition).

Various SA settings, ranging from 0 to 13 CAD before TDC, were applied by performing steps at eight operating conditions. Table 2 summarizes the operating conditions tested. Here, the engine speed, the air mass flow, and the coolant temperature (controlled by varying the coolant flow) were changed to

create diverse knocking conditions. Figure 2 shows the spark advance evolution during an SA step test.

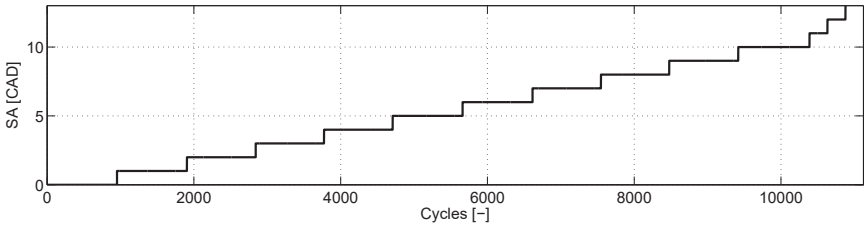

Fig. 2. SA evolution during an example of the steady-state SA steps test

Table 2
Operating conditions

OP	m_{air}^{ref} [g/s]	n [rpm]	T_{cool} ^{o}C
A	25	1500	85
B	22	1500	85
C	25	1500	90
D	22	1500	90
E	19	1250	85
F	16	1250	85
G	16	1250	90
H	19	1250	90

3 Arrhenius-based knock model

As stated above, the autoignition of the end-gas is characterized by the in-cylinder chamber conditions and it can be modelled by an Arrhenius-like function, such as:

$$\tau = C_1 e^{\frac{C_3}{T_{ub}}} p^{C_2} \tag{3}$$

where τ is the ignition delay and T_{ub} are the pressure and temperature of the unburned gasses, respectively, and C_1, C_2 and C_3 are constants defining the autoignition process.

In the present work, the values suggested by Douaud and Eyzat were used [39], namely $C_2 = -1.7$ and $C_3 = 3800$. The model is easily adaptable for a model-based knock control scheme and the only parameter that needs calibration is C_1.

Autoignition is produced when

$$AI = \int_{IVC}^{EOC} \frac{1}{\tau} d\alpha > 1 \tag{4}$$

and the unburned temperature can be calculated by assuming a polytropic process after the spark is produced.

$$T_{ub} = \begin{cases} \frac{pV}{mR} & \text{if } \alpha < SA \\ T_{ub}^{SA} \left(\frac{p}{p^{SA}}\right)^{\frac{\kappa-1}{\kappa}} & \text{otherwise} \end{cases} \tag{5}$$

where κ is the polytropic exponent. In this work, a value of 1.3 was used.

Note that the trapped mass calculated is used in an exponential function, such that, if there was an error in the trapped mass input, it would become in a high deviation at the autoignition delay output.

Figure 3 shows the probability functions of the AI index defined in (4) for four values of SA steps and for all the cycles together, i.e. the steps illustrated in Figure 2. The AI index increases as the spark is advanced because combustion starts closer to TDC provoking higher temperatures of the unburned gas.

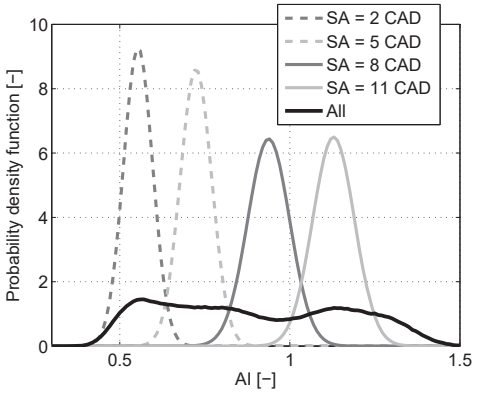

Fig. 3. AI probability functions of various SA steps at point H

Figure 4 shows the knock probability found for the cycles at point H. The

knock probability was calculated by dividing the data in groups of similar AI values, with a resolution of 0.025. Clearly, the knock events are more frequent when the AI index increases, nevertheless, the autoignition hypothesis stated at (4) is not always accomplished, as some cycles with AI values below 1 present knock and others above do not.

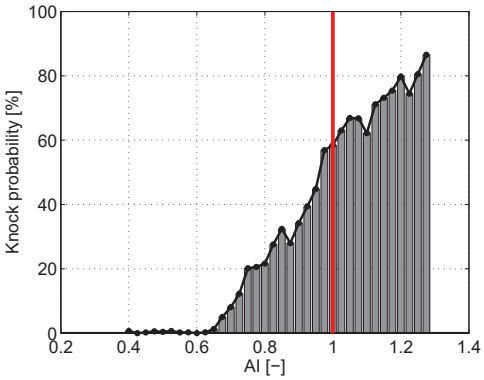

Fig. 4. Knock probability measured as a function of the AI index at point H

4 Exogenous noise and knock probability estimation

Errors at the temperature estimation of the unburned gas preclude a deterministic prediction of knock. These errors can be caused by unobservable effects, e.g. temperature hot spots or residual mass variations, but also by measurement and modelling errors, such as pegging errors or errors at the occurring estimations of the trapped mass and γ.

The present paper proposes the use of an error probability distribution φ_T which is added in the computed unburned gas temperature and which takes into account all the uncertainties in the measurement. This probability distribution is used to calculate, at each cycle, a probability distribution for the autoignition parameter defined in Equation (4), as follows:

$$\varphi_{AI} = AI + \frac{dAI}{dT}\varphi_T \tag{6}$$

where $\frac{dAI}{dT}$ is numerically calculated by:

$$\frac{dAI}{dT} = \frac{AI(T_{ub} + \Delta T, p) - AI(T_{ub}, p)}{\Delta T} \tag{7}$$

Finally, the knock probability can be obtained by integrating the probability that knock occurs:

$$p_{KE} = \int_{AI>1} \varphi_{AI} \tag{8}$$

Following these steps, if the exogenous noise was set to 0, the function of the knock probability would be a digital function. If the noise was a bias in any measurement, this would result in an offset of the final probability function. And if the error was a random function, it would smooth the probability function by having the 50% probability at $AI = 1$. Figure 5 exemplifies the effect of various exogenous noises at the knock probability function by using a constant temperature sensitivity dAI/dT of 0.04.

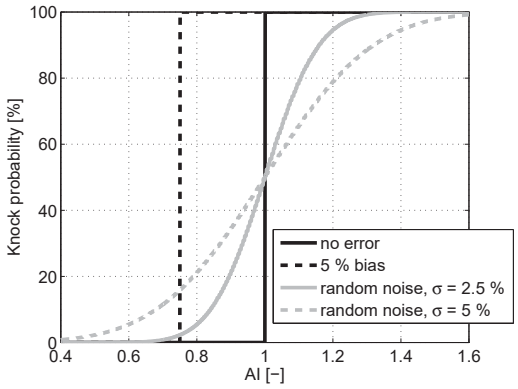

Fig. 5. Effect of various types of errors to the knock probability function

The exogenous noise was chosen to be a normal distribution with 0 mean and constant standard deviation. The standard deviation was calibrated at point H by using the least squares method. The value found was 5.29% and the result of the model is shown in Figure 6.

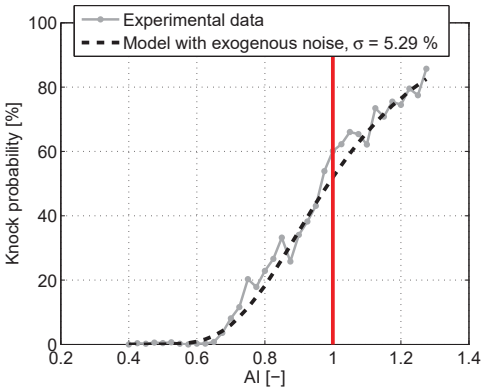

Fig. 6. Effect of various type of errors on the knock probability function

Note that the knock probability shown in Figure 6 is calculated cycle-by-cycle by varying the temperature sensitivity dAI/dT, while the example whown in Figure 5 is computed with a constant temperature sensitivity of 0.04. Figure 7 plots the autoignition parameters for 50 consecutive cycles for each SA value at the point H. It must be noticed that the SA not only strongly influences the autoignition time (AI) calculated, but also the temperature sensitivity.

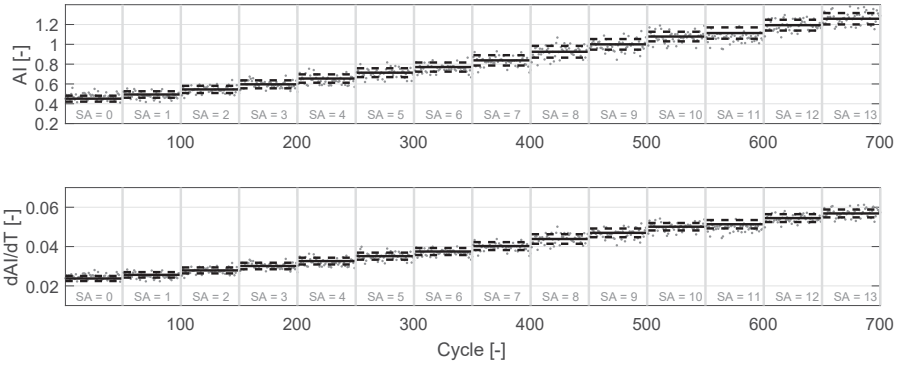

Fig. 7. Autoignition parameter and temperature sensitivity for different SA settings at point H

Figure 8 illustrates the knock probability calculation by plotting the probability function of the AI for four individual cycles with different SA values. The knocking probability is computed by integrating the area above the knocking criteria, which is represented by a dashed line. Note that, the autoignition parameter (AI) determines whether a cycle is knocking or not, i.e. above or below 50% of knock probability, while the temperature sensitivity determines the trust worthiness of this estimation.

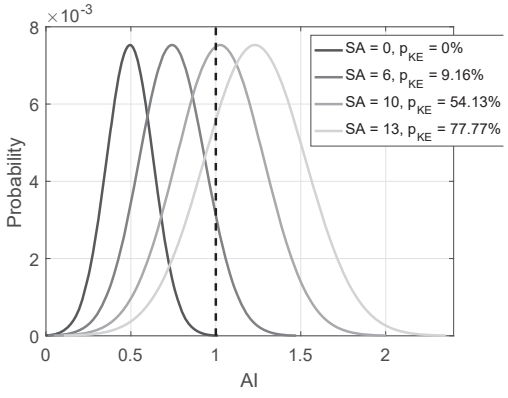

Fig. 8. AI probability distribution computed for four cycles at point H

5 Model Validation

As stated above, the knock model was validated at eight operating conditions, as summarized in Table 2. Each cycle was analysed independently and an exogenous noise with $\sigma = 5.29\%$ was used for all of them. Figure 9 shows the probability density function of AI for each test. Clearly, points G and H have higher values of AI, while points B and D have lower values.

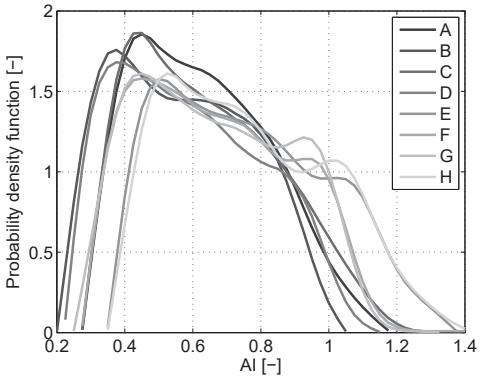

Fig. 9. Probability density functions for each OP

Left plot of Figure 10 shows the results of the knock model when T_{ub} is computed by using the air mass flow sensor for all the operating conditions. The model shows an offset when the operating conditions are varied. This offset is caused by air mass flow sensor errors. If traditional sensors were employed, each operating condition would need a different value of C_1 for dealing with the sensor bias, and the model would require a constant adaptation when transients are performed. Nevertheless, this offset can be corrected by using the pressure resonance of the cylinder for detecting the total mass trapped.

This methodology for inferring the mass trapped from in-cylinder pressure resonance oscillations was recently developed and it is the first time that it is used in conventional SI engines. A more detailed description of the procedure can be found in Appendix A. The right plot of Figure 10 shows the results obtained when the unburned temperature is detected by using the resonant frequencies. Note that all the experimental lines collapse around the predicted value and only a single value of C_1 was required for running the model. This model could be used for knock control by maintaining the AI index at a desired level, e.g. if the AI index was maintained at 0.8, the percentage of knocking cycles would remain below 20%.

The complete model uses the in-cylinder pressure and the geometrical param-

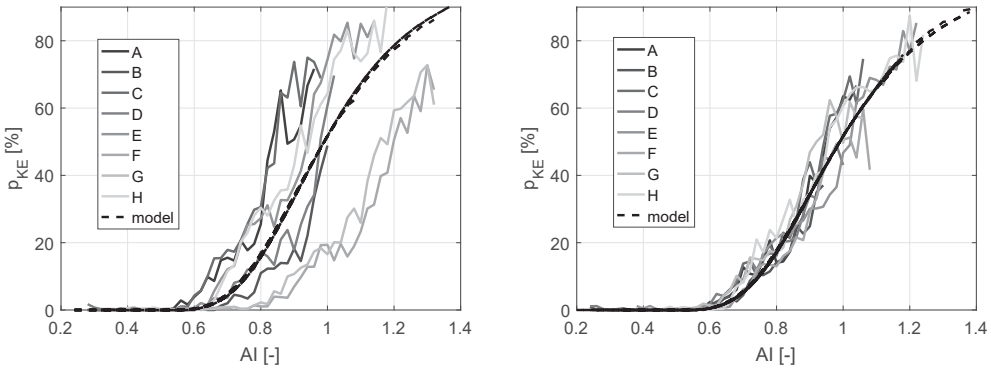

(a) With air mass flow sensor (b) Using pressure resonance

Fig. 10. Knock probability calculation

eters of the engine to estimate the probability of knock. The model can be summarized by the following steps:

(1) The content of the in-cylinder pressure compressed on the frequency band of resonance (between 4 kHz and 20 kHz) is used for characterizing the acoustical waves and estimating the in-cylinder trapped mass.
(2) The low-frequency band of the pressure signal is used to analyse the combustion, compute the temperature of the unburned gases, and estimate the autoignition delay.
(3) An exogenous noise is added to the unburned gas temperature and it is propagated along the model. This yields a probability distribution of the autoignition delay (not a single value).
(4) The knock probability is obtained by integrating the autoignition delay probability distribution which predicts an autoignition of the end-gas before the combustion ends.

Figure 11 shows a scheme of the complete model. Note that the in-cylinder pressure signal is the only input required for computing the knock probability.

6 Conclusions

A knock model was developed for predicting knock probability. The knock probability is calculated by assuming an error probability distribution on the temperature of the unburned gases and propagating this error along a simple knock model based on an Arrhenius-like function. The model uses in-cylinder pressure resonant frequencies to determine the unburned gas temperature. Doing so, sensor bias is avoided and the model does not need to be constantly adapted in transient operation.

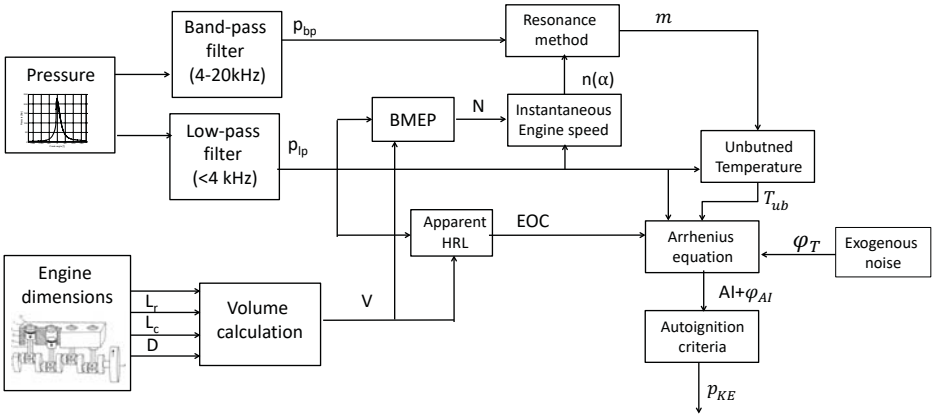

Fig. 11. Model scheme for knock probability estimation

The most important contributions of the model developed are:

- The in-cylinder conditions of the SI engines when knock must be controlled are specially suitable for detecting the resonance phenomenon: High loads excite in-cylinder pressure resonance, the absence of a bowl in SI engines ensures a constant Bessel factor and there is no air after combustion, facilitating the estimation of the gas properties.
- Only the pressure signal is required, which significantly reduces the sources of errors.
- The trapped mass is directly computed, with no need for a residual gas fraction model.
- The model can be adapted by actualizing a single parameter. This is essential for knock models as they must be continuously adapted to deal with any variation, e.g. caused by ageing.

The model was validated in a four-stroke SI engine by varying several knocking conditions; namely spark advance, engine speed, load, and coolant temperature. Results show an important bias when using current sensors for computing the trapped mass. However, the model accurately predicts the knock probability when the trapped mass is obtained from the resonant content of the pressure signal.

A Estimation of the trapped mass

It is possible to determinate the in-cylinder trapped mass from the acoustic characteristics of the pressure waves, caused by the combustion [20, 21]. As known from [31], the evolution of the resonant frequency depends on the

cylinder geometry and the in-cylinder speed of sound, as follows:

$$f_{res}(\alpha) = \frac{a(\alpha)\, B}{\pi D} \tag{A.1}$$

where a is the speed of sound, f_{res} is the resonant frequency, B is the Bessel coefficient for the given resonant mode, D is the cylinder bore and α represents the crank angle evolution.

Hickling et al. were the first authors trying to take advantage of resonance by measuring the oscillation period and estimating the bulk temperature [40]. The approach was adapted by Guardiola et al. for obtaining the trapped mass by using STFT [20, 21]:

$$m = \gamma p V \left(\frac{B}{f_{res} \pi D} \right)^2 \tag{A.2}$$

where p is the in-cylinder pressure, V the instantaneous cylinder volume and γ is the ratio between constant pressure and constant volume heat capacities (c_p/c_v), as shown in Figure A.1:

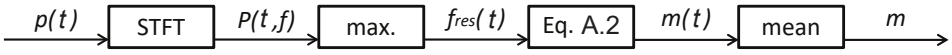

Fig. A.1. Trapped mass calculation by the STFT method

The methodology was finally systematized by developing a specific transformation which implicitly takes into account the resonant frequency evolution [22], thus avoiding time-frequency calculations. Instead of using constant frequency harmonics, this transformation uses time-varying harmonics that depend on virtual masses, such as:

$$S(m) = R[p(t)] = \int_{-\infty}^{\infty} p(t) e^{-j2\pi \int_{-\infty}^{t} \frac{B\sqrt{\gamma(\tau)p(\tau)V(\tau)}}{\pi D\sqrt{m}} d\tau} dt \tag{A.3}$$

The actual trapped mass makes this transformation maximum, and the value of the peak provides information about the strength of that resonant mode. A scheme of the trapped mass estimation procedure that uses the direct transformation is shown in Figure A.2.

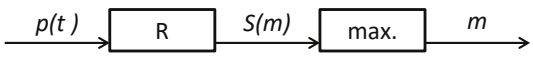

Fig. A.2. Trapped mass calculation by direct transformation

Equation A.3 was discretized and computed from 30 to 80 CAD after TDC, which yields:

$$S(m) = \sum_{\alpha=80}^{\alpha=30} T(\alpha)p(\alpha)e^{-j2\pi \sum_{\phi=0}^{\phi=\alpha} \frac{T(\phi)B\sqrt{\gamma(\phi)p(\phi)V(\phi)}}{\pi D\sqrt{m}}} \tag{A.4}$$

As the engine is closed-loop controlled by a lambda sensor to have stoichiometric conditions, all the gases after combustion are burned products and the value of γ can be computed by a single polynomial equation, such as in [41].

In past works [20, 21, 22], the method was applied to CI engines and a crank-angle-dependent parameter was included to take into account the disturbance associated with the existence of the bowl in the proximity of the TDC and the engine speed fluctuations. Herein, the method is applied for the first time in a conventional SI engine and it was improved by modelling the instantaneous engine speed by using the model proposed by Li and Stone [30]. This model predicts the engine speed fluctuations by modelling the inertial forces of the piston movement. Figure A.3 shows the measured and modelled engine speed for 50 consecutive cycles, at the operating conditions of point A.

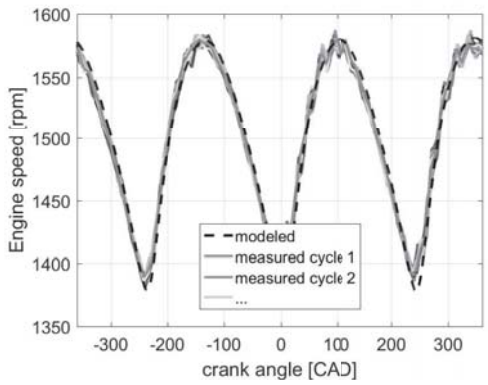

Fig. A.3. Measured and modelled engine speed for 50 consecutive cycles in steady conditions

The inclusion of the engine speed fluctuations into the trapped mass estimations is needed for relying on Draper's equation. Figure A.4 shows one cycle pressure signal (top plot), analysed by WD (medium plot) and by STFT (bottom plot). Herein, the resonance frequency evolution, computed by Equation (A.3), is represented by a dashed line and was calculated for the first radial mode using a constant Bessel factor ($B = 1.842$) and including the engine speed fluctuations in the sampling period ($T = 1/F_s = 1/30n$).

If a constant engine speed is assumed, the frequency shift does not correspond

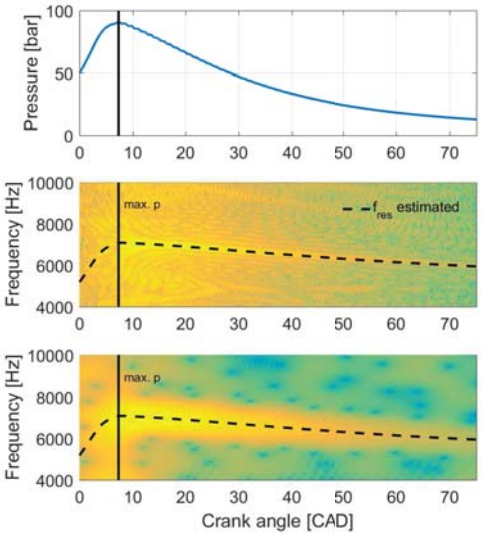

Fig. A.4. Bessel constant found for different crank angle locations

with theory of a cylindrical combustion chamber and a variable Bessel factor is needed. Figure A.5 shows the band-passed pressure signal of Figure A.4 and the Bessel factor evolution identified with and without including the engine speed fluctuations. This coefficient was computed by measuring the trapped mass, computing the speed of sound, and measuring the resonant frequencies (f_{res}), as follows:

$$B(\alpha) = \frac{f_{res}(\alpha)\,\pi D}{a(\alpha)} \tag{A.5}$$

The resonant frequencies f_{res} were identified by using the WD and by selecting the most excited frequency at each crank angle location.

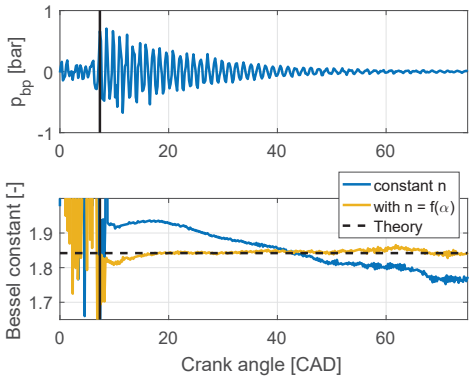

Fig. A.5. Bessel constant found for different crank angle locations

There are two benefits of including the engine speed fluctuations in the calculation. First, there is no need for calibration and the method can be directly used. Second, a crank-angle-dependent calibration, as suggested in previous works, does not take into account the effect of the load at the engine speed fluctuations. The differences at the engine speed between high load and low load can cause errors of up to 2% in the trapped mass calculation for the crank angle range considered.

A.1 Trapped mass results over steady-state tests

The trapped mass was computed from the fuel balance, from the air mass flow sensor, and by using the resonance methodology for all the steady operating conditions listed in Table 2. The RGF was estimated between 2.9% and 3.5% and lambda was maintained near stoichiometric conditions ($m_{air} \approx 14.7 m_{fuel}$). Figure A.6 compares all three methodologies. Measurement data from resonance better fits the measurement results obtained by the fuel balance, and the small discrepancies between them can also be attributed to the λ sensor or to the RGF estimation.

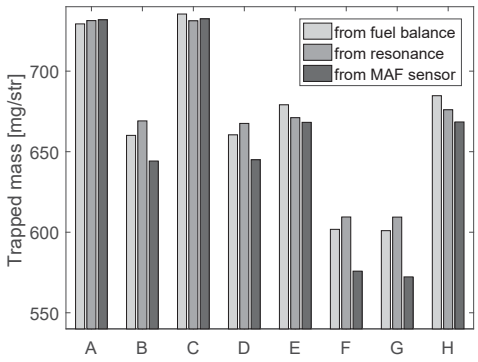

Fig. A.6. Results of trapped mass computations over steady operating points

References

[1] J. B. Heywood. *Internal Combustion Engine Fundamentals*. McGraw-Hill, Inc., 1988.

[2] X. Zhen, Y. Wang, S. Xu, Y. Zhu, C. Tao, T. Xu, and M. Song. The engine knock analysis - an overview. *Applied Energy*, 92:628–636, 2012.

[3] C. Forte, E. Corti, and G. M. Bianchi. Combined experimental and numerical analysis of knock in spark ignition engines. In *Proceedings of the ASME Internal Combustion Engine Division Fall Technical Conference 2009*, pages 473–488, 2009.

[4] J. McKenzie and W. K. Cheng. The anatomy of knock. *SAE Technical Papers*, 2016.

[5] J. C. Peyton Jones, J. M. Spelina, and J. Frey. Likelihood-based control of engine knock. *IEEE Transactions on Control Systems Technology*, 21(6):2169–2180, 2013.

[6] G. Zhu, I. Haskara, and J. Winkelman. Stochastic limit control and its application to spark limit control using ionization feedback. In *Proceedings of the American Control Conference*, volume 7, pages 5027–5034, 2005.

[7] J. M. Spelina, J. C. Peyton Jones, and J. Frey. Stochastic simulation and analysis of a classical knock controller. *International Journal of Engine Research*, 16(3):461–473, 2015.

[8] G. Panzani, C. Onder, and F. Ostman. Engine knock margin estimation using in-cylinder pressure measurements. *IEEE/ASME Transactions on Mechatronics*, 2016.

[9] N. Cavina, G. Po, and L. Poggio. Ion current based spark advance management for maximum torque production and knock control. In *Proceedings of 8th Biennial ASME Conference on Engineering Systems Design and Analysis, ESDA2006*, volume 2006, 2006.

[10] G. Kalghatgi, H. Babiker, and J. Badra. A simple method to predict knock using toluene, n-heptane and iso-octane blends (tprf) as gasoline surrogates. *SAE International Journal of Engines*, 8(2):505–519, 2015.

[11] J. M. Spelina, J. C. Peyton Jones, and J. Frey. Characterization of knock intensity distributions: Part 1: Statistical independence and scalar measures. *Proceedings of the Institution of Mechanical Engineers, Part D: Journal of Automobile Engineering*, 228(2):117–128, 2014.

[12] J. M. Spelina, J. C. Peyton Jones, and J. Frey. Characterization of knock intensity distributions: Part 2: Parametric models. *Proceedings of the Institution of Mechanical Engineers, Part D: Journal of Automobile Engineering*, 227(12):1650–1660, 2013.

[13] E. Galloni. Analyses about parameters that affect cyclic variation in a spark ignition engine. *Applied Thermal Engineering*, 29(5-6):1131–1137, 2009.

[14] F. Bozza, D. Siano, and E. Torella. Cycle-by-cycle analysis, knock modeling and spark-advance setting of a "downsized" spark-ignition turbocharged engine. *SAE International Journal of Engines*, 2(2):381–389, 2010.

[15] R. Schiel and U. Maas. Analysis of endgas temperature fluctuations in an si engine by laser-induced fluorescence. *Combustion and Flame*, 133(1-2):19–27, 2003.

[16] M. Pöschl and T. Sattelmayer. Influence of temperature inhomogeneities on knocking combustion. *Combustion and Flame*, 153(4):562–573, 2008.

[17] N. Kawahara, E. Tomita, and Y. Sakata. Auto-ignited kernels during knocking combustion in a spark-ignition engine. *Proceedings of the Combustion Institute*, 31 II:2999–3006, 2007.

[18] J. C. Livengood and P. C. Wu. Correlation of autoignition phenomena in internal combustion engines and rapid compression machines. *Symposium (International) on Combustion*, 5(1):347–356, 1955.

[19] D. Bradley. Autoignitions and detonations in engines and ducts. *Philosophical Transactions of the Royal Society A: Mathematical, Physical and Engineering Sciences*, 370(1960):689–714, 2012.

[20] C. Guardiola, B. Pla, D. Blanco-Rodriguez, and P. Bares. Cycle by cycle trapped mass estimation for diagnosis and control. *SAE Int. J. Engines*, 7(3), 2014.

[21] J. M. Luján, C. Guardiola, B. Pla, and P. Bares. Estimation of trapped mass by in-cylinder pressure resonance in HCCI engines. *Mechanical Systems and Signal Processing*, 2015. Article in Press.

[22] A. Broatch, C. Guardiola, B. Pla, and P. Bares. A direct transform for determining the trapped mass on an internal combustion engine based on the in-cylinder pressure resonance phenomenon. *Mechanical Systems and Signal Processing*, 62:480–489, 2015.

[23] C. Guardiola, V. Triantopoulos, P. Bares, S. Bohac, and A. Stefanopoulou. Simultaneous estimation of intake and residual mass using in-cylinder pressure in an engine with negative valve overlap. *IFAC-PapersOnLine*, 49(11):461–468, 2016.

[24] C. C. Guardiola, J. Martín, J. Pla, and P. Bares. Cycle by cycle nox model for diesel engine control. *Applied Thermal Engineering*, 110:10111020, 2017.

[25] Z. Liu and C. Wang. An lpv adaptive observer for updating a map applied to an maf sensor in a diesel engine. *Sensors (Switzerland)*, 15(10):27142–27159, 2015.

[26] J. Zhao and J. Wang. Engine mass airflow sensor fault detection via an adaptive oxygen fraction observer. In *Proceedings of the American Control Conference*, pages 1517–1522, 2014.

[27] J. Yang, K. Sata, J. Kako, A. Ohata, and T. Shen. Statistical model and control of residual gas mass in gasoline engines. In *IFAC Proceedings Volumes (IFAC-PapersOnline)*, volume 7, pages 594–599, 2013.

[28] J. Larimore, E. Hellström, S. Jade, A. G. Stefanopoulou, and L. Jiang. Real-time internal residual mass estimation for combustion with high cyclic variability. *International Journal of Engine Research*, 16(3):474–484, 2015.

[29] A. Broatch, C. Guardiola, P. Bares, and F.D. Denia. Determination of the resonance response in an engine cylinder with a bowl-in-piston geometry by the finite element method for inferring the trapped mass. *International Journal of Engine Research*, 2015.

[30] H. Li and B. J. Stone. Time domain modelling of a reciprocating engine. *Mechanical Systems and Signal Processing*, 13(1):169–178, 1999.

[31] C. S. Draper. The physical effects of detonation in a closed cylindrical chamber. Technical report, National Advisory Committee for Aeronautics, 1938.

[32] K. M. Chun and J. B. Heywood. Estimating heat-release and mass-of-mixture burned from spark-ignition engine pressure data. *Combustion Science and Technology*, 54(1-6):133–143, 1987.

[33] S. Wang, R. Prucka, M. Prucka, and H. Dourra. Control-oriented residual gas mass prediction for spark ignition engines. *International Journal of Engine Research*, 16(7):897–907, 2015.

[34] E. A. Ortiz-Soto, J. Vavra, and A. Babajimopoulos. Assessment of residual mass estimation methods for cylinder pressure heat release analysis of hcci engines with negative valve overlap. *Journal of Engineering for Gas Turbines and Power*, 134(8), 2012.

[35] *Time Frequency Signal Analysis*. McGraw Hill, 1996.

[36] A. Chen and X. Dai. Internal combustion engine vibration analysis with short-term fourier-transform. In *Proceedings - 2010 3rd International Congress on Image and Signal Processing, CISP 2010*, volume 9, pages 4088–4091, 2010.

[37] L. Stankovi and J. F. Bhme. Time-frequency analysis of multiple resonances in combustion engine signals. *Signal Processing*, 79(1):15–28, 1999.

[38] P. Bares, D. Selmanaj, C. Guadiola, and C. Onder. A new knock event definition for knock detection and control optimization. *Applied Thermal Engineering*, 2016.

[39] A. M. Douaud and P. Eyzat. Four-octane-number method for predicting the anti-knock behavior of fuels and engines. *SAE Technical Papers*, 1978.

[40] R. Hickling, D. A. Feldmaier, F. H. K. Chen, and J. S. Morel. Cavity resonances in engine combustion chambers and some applications. *Journal of the Acoustical Society of America*, 73(4):1170–1178, 1983.

[41] M. Lapuerta, O. Armas, and J. J. Hernández. Diagnosis of di diesel combustion from in-cylinder pressure signal by estimation of mean thermodynamic properties of the gas. *Applied Thermal Engineering*, 19(5):513–529, 1999.